JOURNAL OF CATALYSIS 149, 438–448 (1994)

n-Butane Hydrogenolysis at Sn/Pt(111) Surface Alloys

János Szanyi,* Shane Anderson,† and Mark T. Paffett

*Chemical Science and Technology Division, LANL, Los Alamos, New Mexico 87545; and †Chemical Engineering Department, University of New Mexico, Albuquerque, New Mexico 87131

Received March 11, 1994; revised July 21, 1994

Ordered bimetallic Sn/Pt(111) surface alloys have been prepared in an ultrahigh vacuum system and used in model moderate pressure (1-200 Torr) batch catalytic reactions. Hydrogenolysis of *n*-butane (H_2/n-C_4 = 100) was conducted on these surfaces to characterize the effects of ordered bimetallic ensembles relative to those available at the Pt(111) surface over the temperature range 525–625 K. For these conditions, specific *n*-butane hydrogenolysis reaction rates were determined for the $p(2 \times 2)$ Sn/Pt(111) surface alloy, the $(\sqrt{3} \times \sqrt{3})$R30° Sn/Pt(111) surface alloy, and Pt(111) as a function of temperature. The order of relative activities is $p(2 \times 2)$ Sn/Pt(111) surface alloy > Pt(111) > $(\sqrt{3} \times \sqrt{3})$R30° Sn/Pt(111) surface alloy with specific activation energies of 29 ± 2 kcal mol^{-1} for all three surfaces below 575 K. A leveling in activity is seen for all three surfaces at temperatures above 575 K. The hydrogenolysis activity of the $p(2 \times 2)$ Sn/Pt(111) surface alloy is approximately 5–6 times greater than that seen over Pt(111) and the $(\sqrt{3} \times \sqrt{3})$R30° Sn/Pt(111) surface alloy is approximately an order of magnitude less active. Product distributions and catalytic deactivation were found to be substantially different for these three surfaces. These results are discussed in terms of the ensemble requirement differences inherent to the hydrogenolysis pathways available at each of the base metals under these conditions of temperature, pressure, and hydrogen/hydrocarbon ratio. © 1994 Academic Press, Inc.

1.0. INTRODUCTION

Bimetallic Group VIII catalysts are commonly used in the processing of petrochemicals (1) with supported Sn/Pt one of the most widely studied compositions. However, the effects of alloying Sn with the Group VIII metals on their catalytic properties are not fully understood. Sinfelt has postulated (1) that ensemble formation during the alloying process leads to enhanced selectivity for hydrocarbon isomerization in preference to the undesired hydrogenolysis reactions in petrochemical reformation. However, a detailed molecular description of the chemical reactions based on the specific bimetallic ensemble formation has not been elucidated. In this study, the formation of contiguous metal atom ensembles on the (111) face of Pt through thermal annealing of ultrathin Sn deposits will be reviewed in the context of their chemical reactivity toward *n*-butane hydrogenolysis at specific conditions of temperature, partial pressures, and reactant ratios. The intent is to use these designed surfaces to tailor reaction chemistry specific to the ensemble required for this hydrocarbon conversion chemistry.

Recently, the preparation and UHV surface science characterization of Sn/*M*(111) and Sn/*M*(100) (*M* = Ni, Pt, Pd) single crystal surface alloys have been accomplished (2–6). The procedure for characterization of these bimetallic surfaces is to vapor-deposit a specific initial concentration of Sn onto a specific single crystal substrate and to then follow the resultant surface stoichiometry and order as a function of annealing temperature using surface specific probes such as Auger electron spectroscopy (AES), low energy electron diffraction (LEED), and low energy ion surface scattering (LEISS). Because of the inherently low surface free energy of Sn (and low melting temperature) in comparison to the Group VIII transition metal surfaces (2), the Sn adatoms diffuse across the surface and remain segregated at the outermost surface of the substrate. In addition, the formation of intermetallic compounds and ordered surface alloys is thermodynamically favorable (7, 8) at a high enough temperature. In all cases studied to date (e.g., the (100) and (111) faces of Pd, Ni, and Pt), the Sn vapor deposition and annealing step has produced ordered surface alloys in which the Sn adatoms are located approximately in the plane of the substrate surface (as opposed to an ordered metal overlayer). The extent of Sn atom protrusion or surface rippling is measurably different for starting metallic substrates, with the greatest effect observed in systems with the most disparate metallic radii. For example, explicit ion surface scattering determinations for Sn adatom rippling at the $(\sqrt{3} \times \sqrt{3})$R30° Sn/Pt(111) and $(\sqrt{3} \times \sqrt{3})$R30° Sn/Ni(111) systems have revealed that the Sn adatoms protrude from the substrates surface plane 0.22 and 0.43 Å, respectively (2, 6).

The hydrogenolysis of butane was chosen as a prototypical reaction for assessing the role of ordered ensembles because of the large literature base (for example see Refs.

0021-9517/94 $6.00

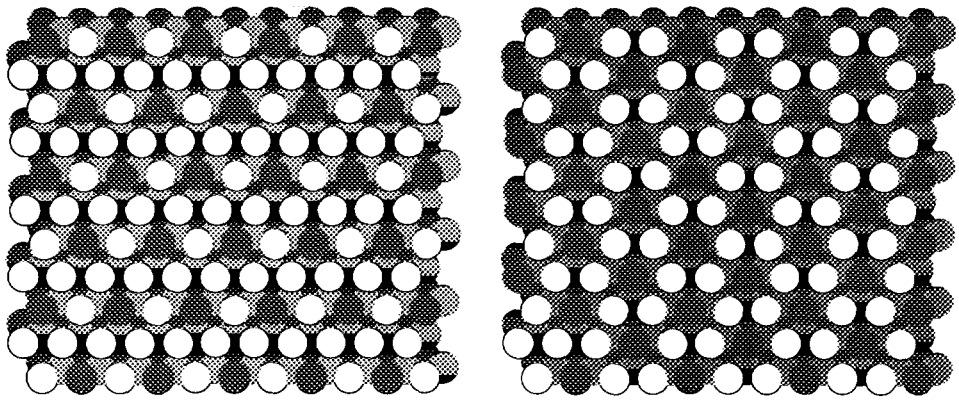

FIG. 1. Real space representation of the $p(2 \times 2)$ (left) and $(\sqrt{3} \times \sqrt{3})$R30° Sn/Pt(111) surface alloys (right). In the outermost layer the tin atoms are dark and the platinum atoms are light.

(9–11) and references contained therein) covering chemical reactivity on both supported catalysts and single crystals. Furthermore, the reactions of hydrocarbons are well known to be structurally sensitive at the third row group VIII transition metals with differing reactivities and selectivities observed at different crystalline faces. A specific example emphasizing the structure sensitivity of *n*-butane hydrogenolysis is the work of Engstrom *et al.* (12) at Ir(111) and Ir(110) surfaces. In contrast to this surface sensitive reactivity, recent measurements of *n*-butane hydrogenolysis by Datye *et al.* (13) indicated relatively little difference in activity between the three low index surfaces of Rh. Structural determinations of the $(\sqrt{3} \times \sqrt{3})$R30° Sn/Pt(111) and $p(2 \times 2)$ Sn/Pt(111) surface alloys have revealed that for each of these surfaces Pt atoms have three and four in-plane nearest Pt neighbors, respectively (Fig. 1). All threefold hollow Pt sites have been removed at the $(\sqrt{3} \times \sqrt{3})$R30° Sn/Pt(111) surface alloy and 50% eliminated in the $p(2 \times 2)$ Sn/Pt(111) surface alloy. Therefore, it is postulated that this subtle difference in availability of Pt surface atoms may translate into notable variations in reactivity with respect to hydrocarbon reactions. This work examines these reactivity differences in terms of ensemble requirements for *n*-butane hydrogenolysis. Preliminary reports (14) of the hydrogenolysis activity observed at the $(\sqrt{3} \times \sqrt{3})$R30° Sn/*M*(111) (*M* = Ni, Ph, Pt) surface alloys indicated a notable decrease in overall *n*-butane hydrogenolysis activity when compared to the clean *M*(111) starting templates. In addition, the $(\sqrt{3} \times \sqrt{3})$R30° Sn/M(111) (*M* = Ni, Pt) (14) surface alloys have been noted to exhibit considerably less carbon buildup under reaction conditions when compared to the clean (111) metal surfaces.

2.0. EXPERIMENTAL

Experiments were carried out in a combined UHV surface analysis-elevated pressure microreactor system. The UHV chamber is equipped with AES, XPS, LEED, TDMS, and inert gas LEISS characterization capabilities that has been described in detail before (4, 15). Surface preparation and characterization of the specific $p(2 \times 2)$ and $(\sqrt{3} \times \sqrt{3})$R30° Sn/*M*(111) surface alloys are fully discussed elsewhere (4, 6). Briefly, the clean Pt(111) was prepared by cycles of room temperature neon ion sputtering and oxidation at 800 K followed by an anneal at 1200 K. The Sn/Pt(111) surface alloys were prepared by the deposition of Sn on the clean Pt(111) surface followed by a brief anneal at 1000 K. The hydrogenolysis and isomerization activation energies were determined for the single crystals and the Sn/Group VIII surface alloys at total pressures from 50.5 to 100.5 Torr and $H_2/n\text{-}C_4$ ratios from 20 to 200. The hydrogenolysis activity was determined by quantitatively measuring product distributions following batch reactor catalytic runs using gas chromatography (GC). A Porapack Q column was used for gas separations (operated at 373 K) with GC detector sensitivity factors determined from a reference gas mixture (Scott Speciality no. 220 C_1–C_6 alkane mixture in Ar). Specific reaction rates expressed as turnover frequencies (TOF-product molecules per surface atom per second) were determined using the formula

$$\text{TOF} = \frac{(V_{\text{rctr}})(P_{n\text{C4}})[6.023 \times 10^{23}][X_{n\text{C4}}]}{(R)(293\ \text{K})[t_{\text{rxn}}][\Theta_{\text{Pt}}]}, \qquad [1]$$

where V_{rctr} is the volume of the reactor (404 ml), $P_{n\text{C4}}$ is the partial pressure of *n*-butane, R is the ideal gas constant, 293 K is the temperature of the reactor, $X_{n\text{C4}}$ is the net *n*-butane conversion (fraction), t_{rxn} is the reaction time in seconds, and Θ_{Pt} is the number of surface sites (one face) of the crystal based upon geometric area measurement (±10%). Activities reported are based on the initial number of metal atoms for the Pt(111) surface (1 mono-

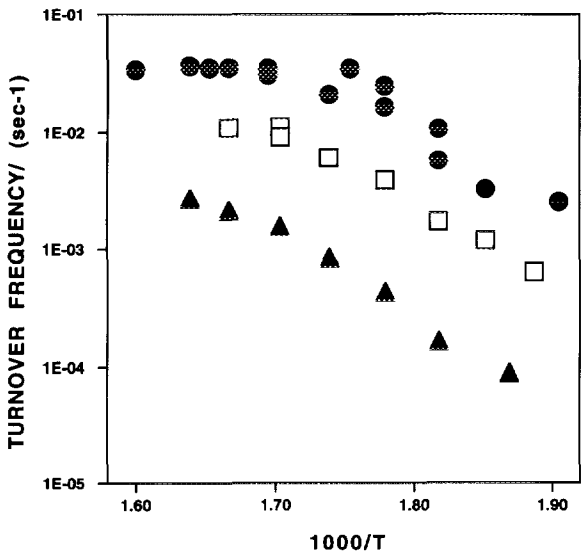

FIG. 2. n-Butane hydrogenolysis activity at Pt(111) (□), the $p(2 \times 2)$ Sn/Pt(111) surface alloy (●), and the $(\sqrt{3} \times \sqrt{3})R30°$ Sn/Pt(111) surface alloy (▲). The reactant partial pressures were 0.5 Torr for n-butane and 50 Torr for H_2.

layer (ML) = 1.505×10^{15} atoms/cm^2). Activity results for the surface alloys are in relation to the respective single crystals from which they are derived and no normalization for exposed Pt atoms has been applied in the graphed results that follow. All activity results are those based upon initial activities (i.e., less than 2% total conversion of n-butane).

3.0. RESULTS

As a direct test of a model catalytic reaction designed to explore the effect of specific surface ensembles, the hydrogenolysis of n-butane over the $p(2 \times 2)$ Sn/Pt(111) surface alloy and the $(\sqrt{3} \times \sqrt{3})R30°$ Sn/Pt(111) surface alloy were examined in comparison to Pt(111). Shown in Fig. 2 are Arrhenius plots for the n-butane hydrogenolysis reaction with $P_{C4} = 0.5$ Torr and $P_{H2}/P_{C4} = 100$ over the three surfaces and represent initial activities (<2% reactant conversion). The activation energy of the reaction was calculated to be 29 ± 2 kcal mol^{-1} for all surfaces below 575 K. The TOF values shown in Fig. 2 are taken in reference to the starting Pt(111) surface atom density (e.g., $p(2 \times 2)$ and $(\sqrt{3} \times \sqrt{3})R30°$ Sn/Pt(111) surface alloy results have not been corrected according to the displacement of Pt atoms by Sn atoms as shown in Fig. 1). Note that the activity of the $(\sqrt{3} \times \sqrt{3})R30°$ Sn/Pt(111) surface is approximately an order of magnitude lower and that the $p(2 \times 2)$ Sn/Pt(111) surface is substantially (~5X) higher than the Pt(111) surface.

In addition to the noticeable variation in activities among the Sn/Pt(111) surface alloys, the selectivity that each surface exhibits reveals interesting differences in behavior. Shown in Figs 3a–c are the selectivities towards methane, ethane, and propane formation as a function of temperature for each of the three surfaces. In all cases the initial reactant pressures were 0.5 Torr n-butane and 50 Torr hydrogen. In general, the methane selectivities were highest at the highest reaction temperatures and the selectivity toward ethane and propane inversely tracked the methane. The Pt(111) surface exhibited the highest selectivity for methane and propane production, with methane steadily increasing with temperature and propane correspondingly decreasing with increasing temperature. Among the three surfaces, the $p(2 \times 2)$ surface alloy exhibited the lowest methane selectivity and highest ethane production at any given temperature. In comparison to the Pt(111) surface, where the ethane selectivity ranged from 22–30% over the temperature range 537–610

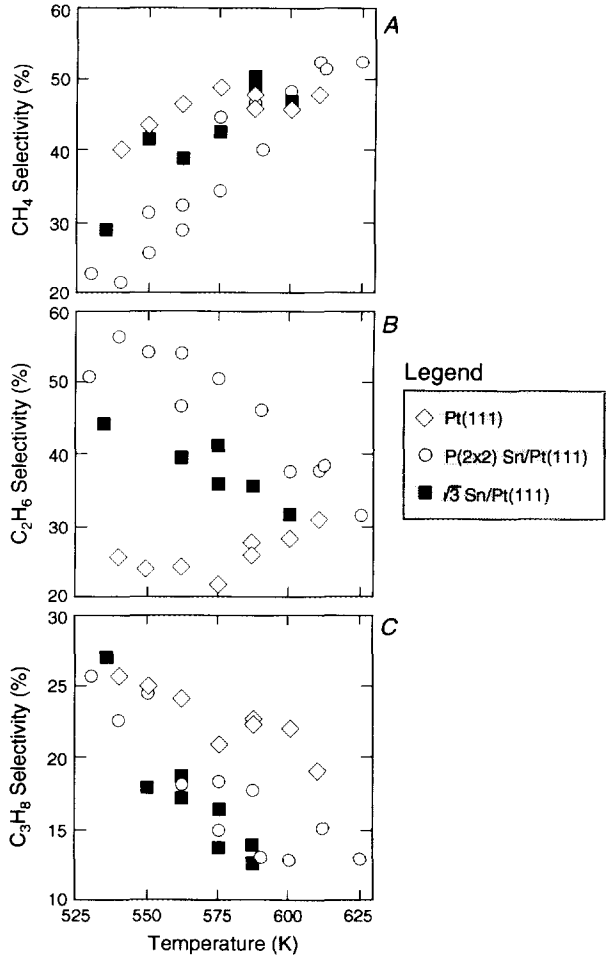

FIG. 3. (A) Methane, (B) ethane, and (C) propane selectivities (mol%) versus temperature for n-butane hydrogenolysis at Pt(111), the $p(2 \times 2)$ Sn/Pt(111) surface alloy, and the $(\sqrt{3} \times \sqrt{3})R30°$ Sn/Pt(111) surface alloy. Reactant partial pressures were the same as in Fig. 2.

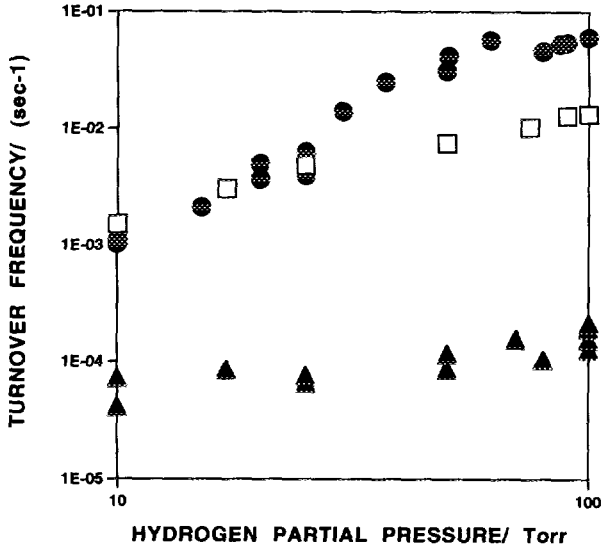

FIG. 4. Hydrogen partial pressure dependence versus turnover frequency for *n*-butane hydrogenolysis at Pt(111) (□), the $p(2 \times 2)$ Sn/Pt(111) surface alloy (●), and the $(\sqrt{3} \times \sqrt{3})$R30° Sn/Pt(111) surface alloy (▲). The temperature was 575 K and the *n*-butane partial pressure was 0.50 Torr.

K, the $p(2 \times 2)$ Sn/Pt(111) surface alloy produced up to 55% ethane at 537 K with the selectivity linearly falling off to 30% at 625 K. For the $(\sqrt{3} \times \sqrt{3})$R30° Sn/Pt(111) surface the ethane selectivity started at 45% at 535 K and linearly decreased to 30% at 600 K. Concomitant with the decrease in ethane selectivity at both Sn/Pt(111) alloys the selectivity toward methane increased with increasing temperature. The general observation of increasing methane production and decreasing ethane and propane production with increasing temperature suggests that multiple hydrogenolysis (C–C cleavage) steps are taking place at higher temperatures.

The hydrogenolysis activity was observed to be very strongly dependent on hydrocarbon to hydrogen ratio for two of the three surfaces. In Fig. 4 the TOFs for *n*-butane hydrogenolysis with 0.5 Torr *n*-butane at 575 K are plotted versus hydrogen partial pressure for the three surfaces. The total pressure was constrained to be 100.5 Torr by adding Ne at all but the highest hydrogen pressures. Note that for the least reactive surface, the $(\sqrt{3} \times \sqrt{3})$R30° Sn/Pt(111) surface alloy, the hydrogen dependence was very small (slope = +0.4). For Pt(111) and the $p(2 \times 2)$ Sn/Pt(111) surface alloy the order with respect to hydrogen pressure dependence were respectively, +0.8 and +1.6. At the lower ratios of hydrogen to *n*-butane the overall activity of the $p(2 \times 2)$ Sn/Pt(111) surface alloy and Pt(111) was observed to be essentially identical. For hydrogen to *n*-butane ratios of ≥ 40 the $p(2 \times 2)$ Sn/Pt(111) surface was observed to be dramatically more active than Pt(111).

In addition to the marked differences in overall activity as a function of hydrogen partial pressure, the selectivities were also observed to vary substantially. The influence of hydrogen partial pressure on the selectivities of the three surfaces are shown in Figs. 5a–c. Note that the predominant product over Pt(111) and $(\sqrt{3} \times \sqrt{3})$R30° Sn/Pt(111) surface alloy is methane at 575 K, and that with an increase in hydrogen partial pressure this product selectivity strongly increases. For the $p(2 \times 2)$ Sn/Pt(111) surface alloy the predominant product is ethane and that the selectivity for this product also increases as the hydrogen partial pressure increases. For Pt(111), the increase in methane selectivity comes at the expense of both ethane and propane. For the $(\sqrt{3} \times \sqrt{3})$R30° Sn/Pt(111) surface alloy the increase in methane selectivity versus hydrogen partial pressure is achieved, in general, at the expense of ethane selectivity. For the $p(2 \times 2)$ Sn/Pt(111) surface

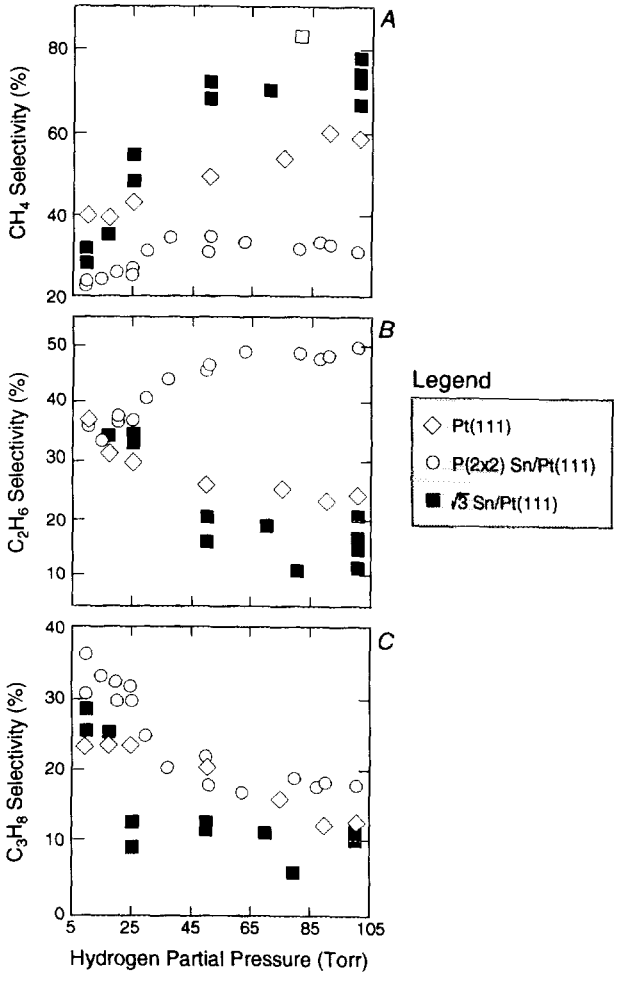

FIG. 5. (A) Methane, (B) ethane, and (C) propane selectivities (Mol%) versus hydrogen partial pressure for *n*-butane hydrogenolysis at Pt(111), the $p(2 \times 2)$ Sn/Pt(111) surface alloy, and the $(\sqrt{3} \times \sqrt{3})$ R30° Sn/Pt(111) surface alloy. The temperature was 575 K and the *n*-butane partial pressure was 0.50 Torr.

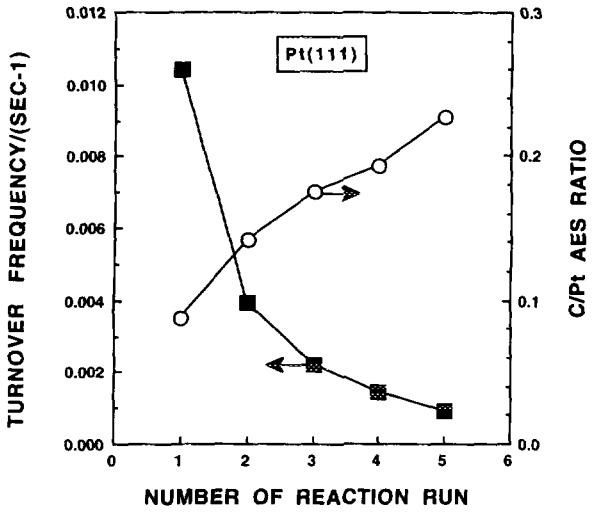

FIG. 6. Deactivation of *n*-butane hydrogenolysis at Pt(111) plotted as turnover frequency versus run number. Sample was not cleaned between batch catalytic runs. Inset: Auger peak-to-peak height ratio for the C(272eV) and Pt(64eV) transistions recorded postreaction. The temperature was 575 K and the reactant partial pressures were 0.50 Torr for *n*-butane and 50.0 Torr for hydrogen.

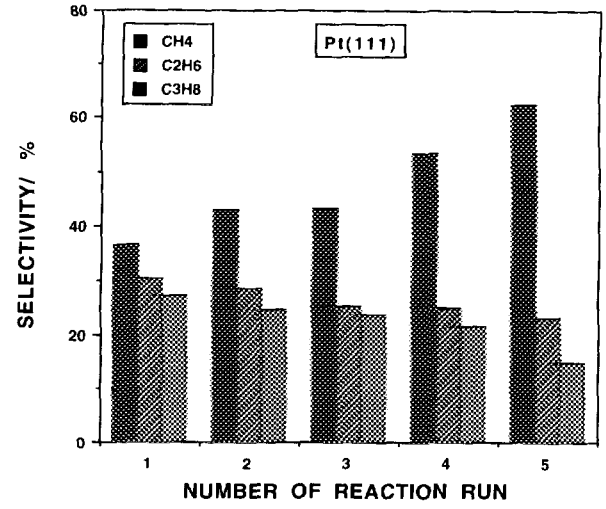

FIG. 7. Product selectivity (mol%) for *n*-butane hydrogenolysis at Pt(111) plotted as turnover frequency versus run number. Same experimental conditions as in Fig. 6.

alloy the increase in ethane selectivity as a function of increasing hydrogen partial pressure is achieved at the expense of a decrease primarily in the selectivity of propane. The $(\sqrt{3} \times \sqrt{3})R30°$ Sn/Pt(111) surface alloy has a comparatively low (10%) and invariant selectivity toward propane under these conditions.

The hydrogenolysis on *n*-butane over Pt(111) and the $p(2 \times 2)$ Sn/Pt(111) surface alloy was noted to be sensitive to poisoning by carbon buildup. In Fig. 6 the TOF for *n*-butane hydrogenolysis at 575 K is plotted for successive batch reaction runs on Pt(111). Following each batch reactor catalytic run the sample was transferred back into the UHV chamber for postreaction AES analysis. The catalyst was first flashed to reaction temperature and an Auger spectrum was recorded. The results of the postreaction surface analysis, expressed as C/Pt Auger signal ratios, are also shown in Fig. 6. Using the calibration of Sachtler and Somorjai (30) an approximate C coverage of 0.35 ML can be determined after the fifth reaction run. The analysis of the shape of the carbon Auger signal also suggests that the form of carbonaceous deposites present on the surface after catalytic measurement is primarily graphitic. Undoubtedly some hydrogen is present in the carbonaceous deposit but it was not quantified. Note that concurrent with the increase in C buildup, as evidenced from the Auger data, a decrease in reactivity is also immediately apparent. In Fig. 7 the corresponding changes in product selectivities are plotted versus reaction run number and demonstrate the marked changes in product distribution as the surface C contamination builds up. The methane selectivity increases as the TOF decreases and the C contamination increases. Accordingly, the ethane and propane fractions decrease with the number of successive reaction runs at the Pt(111) surface. For the $p(2 \times 2)$ Sn/Pt(111) surface alloy the same series of repetitive batch reactions were carried out and the TOF is plotted versus run number in Fig. 8. In comparison to the results observed for Pt(111) in postreaction surface analysis, only a very small (<0.10 that seen at Pt(111)) C Auger signal was observed and it did not increase in magnitude with the number of successive reactions. Postreaction LEED

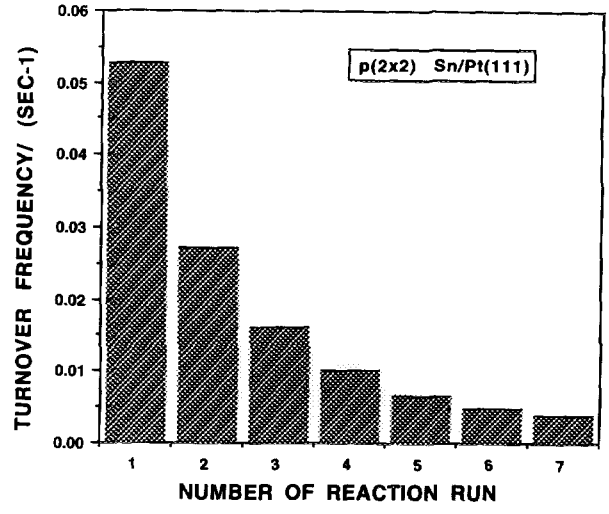

FIG. 8. Deactivation of *n*-butane hydrogenolysis at the $p(2 \times 2)$ Sn/Pt(111) surface alloy plotted as turnover frequency versus run number. Sample was not cleaned between batch catalytic runs. Same experimental conditions as in Fig. 6.

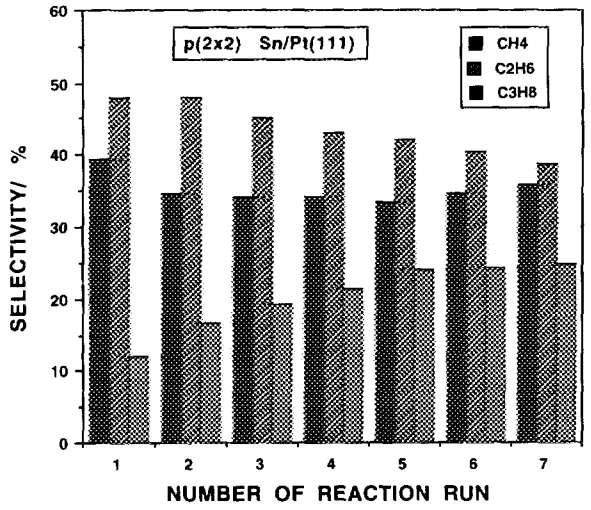

FIG. 9. Product selectivity (mol%) for *n*-butane hydrogenolysis at the $p(2 \times 2)$ Sn/Pt(111) surface alloy plotted as turnover frequency versus run number. Same experimental conditions as in Fig. 6.

examination of the surface did, however, reveal that a mixture of $p(2 \times 2)$ and $(\sqrt{3} \times \sqrt{3})R30°$ domains were present on the surface. The most likely scenario occuring after repetitive reactions at the $p(2 \times 2)$ Sn/Pt(111) surface alloy is that portions of the surface have compressed to form a certain, undetermined fraction of additional $(\sqrt{3} \times \sqrt{3})R30°$ domains. These additional $(\sqrt{3} \times \sqrt{3})R30°$ domains possess an inherently lower reactivity (see Fig. 1) and coupled with the possibility of additional Pt(111) domains arising from compression of Sn into the $(\sqrt{3} \times \sqrt{3})R30°$ domains the Pt (111) domains would more rapidly poison due to C buildup. Therefore, the global kinetic effects (summation of reactivity over entire surface) of multiple distinct domains may lead to several deactivation routes for successive batch reactions at the $p(2 \times 2)$ Sn/Pt(111) surface alloy. In Fig. 9 the corresponding product selectivities are shown for successive batch reactions at the $p(2 \times 2)$ Sn/Pt(111) surface alloy. In comparison to the strong increase in methane selectivity observed at Pt(111) during deactivation, the predominant product, ethane, is less influenced by surface changes following successive batch reaction runs. In fact, the propane selectivity was noted to increase from ~10 to 23% after the seventh consecutive batch reaction with ethane selectivity decreasing from 48 to ~40%.

4.0. DISCUSSION

A. Activities and Selectivities of Pt(111) and Sn/Pt(111)

Significant differences in *n*-butane hydrogenolysis activities were observed for the three different surface compositions. As Fig. 2 shows the most active catalyst for *n*-butane hydrogenolysis under the experimental conditions applied is the $p(2 \times 2)$ Sn/Pt(111) alloy system, followed by the clean Pt(111) and the least active is the $(\sqrt{3} \times \sqrt{3})R30°$ Sn/Pt(111) alloy. The TOF for the clean Pt(111) surface at 573 K is in reasonable agreement with the values reported by Davis *et al.* (16) for a Pt(111) single crystal and Bond *et al.* (17) for EUROPT-1, a silica-supported Pt catalyst. The slight differences in TOFs can be accounted for by the very different reaction conditions applied in these three studies. Hydrogenolysis reactions are noted to be very sensitive to hydrogen partial pressure and hydrocarbon to hydrogen ratio (16, 17). From inspection of Fig. 2 deviations from linearity in the Arrhenius plots are observed for all three catalyst surfaces. Similar observations have been reported previously by others (12, 17–20) for hydrogenolysis reactions for several alkanes and catalysts. The activation energy obtained from the linear part of the Arrhenius plots is 29 ± 2 kcal/mol, approximately the same for all three catalyst surfaces. This value is also in good agreement with earlier published ones for different Pt catalysts (17, 18, 21). The more active the catalyst (high TOF) the lower the reaction temperature where the deviation of the Arrhenius plot from linearity takes place. The accumulation of surface carbonaceous species cannot account for this deviation from linearity. Postreaction AES analysis showed significant carbon level only on the surface of Pt(111) catalyst. If the carbonaceous deposits were responsible for the observed leveling off of the TOF, the only catalyst which would be expected to show this behavior is the Pt(111). Furthermore, if the leveling off is caused by the decreasing number of reaction sites available on the surface of the catalyst due to carbon deposit buildup, we should observe a maximum in activity followed by a steady decrease in activity as the temperature is increased. Negligible carbonaceous deposits are seen on the two Sn/Pt(111) surface alloys following reaction; therefore, another reason must account for the leveling in activity above a certain reaction temperature (which is most apparent for the p(2 × 2) Sn/Pt(111) surface). Bond *et al.* (18) explained the deviation of the Arrhenius plot from linearity by a net decrease in the rate-limiting step resulting from a decrease in the concentration of an adsorbed intermediate with increasing reaction temperature. This explanation might be valid in our case as well. Among hydrocarbon reactions hydrogenolysis is considered one of the more demanding reactions in that it requires a relatively large number of active metal centers (ensembles) and strong hydrocarbon fragment adsorption. The hydrocarbon has to dissociatively adsorb on the surface by cleaving an unspecified number of C–H bonds. For C–C bond breaking to subsequently occur both carbon atoms have to adsorb in such a manner that at least one of them forms a multiple metal–carbon

bond, which in turn provides sufficient strain on the C–C bond (18). *n*-Butane is known to reversibly adsorb (22) on the clean Pt(111), the $p(2 \times 2)$, and the $(\sqrt{3} \times \sqrt{3})$ R30° Sn/Pt(111) surface alloys. In addition, dissociative adsorption of alkanes on close-packed faces of the catalytically important transition metals Ni, Rh, Ir, and Pt is known to occur with a very low probability ((23) and references contained therein). Of relevance to this study, we postulate that by increasing the reaction temperature in the presence of hydrogen the concentration of the dissociatively adsorbed alkane intermediate drops, resulting in a decrease in activity.

The catalytic reactivity with respect to *n*-butane hydrogenolysis becomes more complex at the $p(2 \times 2)$ Sn/Pt(111) surface alloy. There are three main factors to be considered at this ordered surface alloy: (i) changes in surface composition (stoichiometry), (ii) changes in the electronic states of the surface Pt atoms, and (iii) changes in surface morphology. Let us discuss these three factors separately. The $p(2 \times 2)$ Sn/Pt(111) alloy system has a nominal surface composition of Pt_3Sn which corresponds to a $\Theta_{Sn} = 0.25$ (Fig. 1). For this surface structure each Pt atom has four nearest-neighbor Pt atoms in the surface plane (4, 6). There are several arrangements of contigous Pt atoms (ensembles) available on this surface. The most obvious ensembles consist of three and five contiguous Pt atoms. An important feature of this surface structure is the presence of threefold hollow sites which may play a crucial role in hydrogenolysis reactions. The modification of the electronic properties of the surface Pt atoms is brought about by a charge transfer from the Sn toward the Pt atoms. The modification of the electronic properties of surface Pt atoms by the addition of a small amounts of Sn is well documented for both supported (24–27) and single crystal (28) Sn/Pt systems. This effect manifests itself in notably decreased bond strengths for alkenes. The adsorption of ethylene, for example, was shown to be weakened by ~2.5 kcal/mol on this $p(2 \times 2)$ Sn/Pt(111) surface compared to the clean Pt(111) (28). For alkanes the effect is less pronounced but still very apparent with *n*-butane adsorption bond strengths decreasing ~10%. A decrease in the strength of hydrocarbon adsorption has been demonstrated for supported Sn/Pt systems and weakened metal–carbon bonding was suggested to be responsible for the decreased extent of catalyst deactivation through coke formation. The charge donation from Sn toward Pt also influences the adsorption of hydrogen on the catalyst surface. It has been shown (4) that the deposition of Sn on the Pt(111) surface increases the activation energy for hydrogen desorption. The higher affinity of the tin-containing surface toward hydrogen may well result in an increased interaction of hydrogen atoms derived from the hydrocarbon molecule and the surface Pt atoms. This interaction can enhance the weakening of C–H bonds and thus the formation of multiple metal–carbon bonds. The third factor influencing surface reactivity is surface rippling (e.g., corrugation of the Sn/Pt(111) surface alloy). The atomically smooth close-packed Pt(111) surface becomes buckled as Sn atoms place exchange for the surface Pt atoms in forming the surface alloy. The origin of the surface rippling is the difference in atomic radii between Pt and Sn (1.4 and 1.6 Å, respectively) and helps to relieve the strain created by the incorporation of the larger Sn atoms into the Pt(111) surface layer (2, 6). For the Sn/Pt(111) surface alloys the buckling is 0.22 Å. Roughening of the originally atomically smooth Pt(111) surface can have significant consequences for the adsorption and thus the catalytic properties of the Sn/Pt(111) surface alloys. We suggest that the C–H bonds on the carbon atoms adsorbed on the metal surface are strained by the neighboring buckled Sn atoms. This strain can also contribute to the enhanced C–H bond breaking and thus to the increased metal–carbon multiple bond formation. Vibrational spectroscopic measurements of hydrocarbon fragments derived from alkyl and alkenyl species would provide an interesting test of this hypothesis.

In examining the $(\sqrt{3} \times \sqrt{3})$R30° Sn/Pt(111) surface alloy with $\Theta_{Sn} = 0.33$ (surface composition corresponding to Pt_2Sn) the overall catalytic activity toward *n*-butane hydrogenolysis significantly decreases. In this structure all the threefold hollow adsorption sites are eliminated and each surface Pt atom has only three other Pt atom neighbors in the surface layer. The carbon atoms of a hydrocarbon molecule can adsorb only to two Pt atoms in a bridging configuration or to one Pt atom in an a-top position. This site blocking effect can decrease both the concentration of adsorbed *n*-butane molecules and the strength of adsorption between the *n*-butane molecule and the Pt metal atoms (22). We propose that the dramatic decrease in activity is caused mainly by this geometric effect of Sn addition to Pt(111). The same activation energy determined for all three surfaces suggests that the rate-limiting step is the same regardless of the surface composition and is most probably C–C bond breaking.

The selectivity patterns for *n*-butane hydrogenolysis over the three surfaces studied are very different. For Pt(111), CH_4 is produced with the highest selectivity over the entire temperature range studied. Even at the lowest reaction temperature the methane selectivity is higher than that of the statistical product distribution (which assumes equal probability for the rupture of each C–C bond giving 0.33 each methane, ethane, and propane). This observation is somewhat in contrast with the results of Davis *et al.* (16) who found a statistical product distribution for *n*-butane hydrogenolysis over Pt(111) at a reaction temperature of 573 K. However, notably different reaction conditions used in the two studies is an important difference. In Ref. (16) the *n*-butane/hydrogen ratio was

1 : 10 whereas in our study this ratio was 1 : 100. They also observed a large proportion of the reaction proceeding through isomerization and dehydrogenation with considerably more surface C buildup. In the present study, only trace amounts of isomerization products were observed with relatively low surface C buildup ($\Theta_C < 0.3$ ML). The *n*-butane hydrogenolysis product selectivity pattern over Pt(111) reflects the strong adsorption of *n*-butane alkyl fragments on the clean Pt(111) surface. The high methane and low propane selectivity suggest that the adsorbed *n*-butane molecule undergoes multiple C–C bond breaking. This product distribution also suggests that a majority of the *n*-butane molecules are initially adsorbed on the Pt(111) surface through the 1,2-carbon atoms which results in the preferential breaking of the terminal C–C bond. Breaking the terminal C–C bond of *n*-butane would create adsorbed species, CH_x and C_3H_y. The hydrogenation of surface CH_x species would result in the formation of CH_4, which immediately desorbs into the gas phase as methane. The surface C_3H_y species can further react in two different manners. It can be hydrogenated off from the surface producing propane or undergo further hydrogenolysis. On the clean Pt(111) surface, because of the strong adsorption of the C_3H_y species, multiple hydrogenolysis of these adsorbed entities is dominant. We propose that the source of almost the entire C_2H_6 produced is the further hydrogenolysis of these surface C_3H_y species. The hydrogenolysis of the C_3H_y surface entity gives CH_z and C_2H_v species which are successively hydrogenated and desorb as methane and ethane. Under the experimental conditions applied (high H_2/*n*-butane ratio) the adsorbed C_2H_v species is suggested to desorb as C_2H_6 rather than undergo further C–C bond breaking. On clean Ni surfaces, however, the C–C bond breaking sequence produces predominately methane, presumably due to the very strong adsorption of alkyl fragments (23). Over the Pt(111) surface as the reaction temperature increases the selectivity toward methane formation increases up to ~580 K and concomitantly the propane selectivity decreases. In this temperature range the selectivity for ethane formation is essentially unchanged. At temperatures above 580 K the methane slectivity stays at a constant level while the propane selectivity drops and the ethane selectivity increases. At these higher temperatures the accumulation of surface carbonaceous species becomes more pronounced and correspondingly alters the product selectivity. On this partially carbon-covered, poisoned surface the internal C–C bond breaking of the adsorbed *n*-butane molecule appears to be more facile than on the clean Pt(111) surface and accounts for the higher observed ethane selectivity. Summarizing the selectivity results for the two Sn/Pt(111) alloy surfaces we see that for the $p(2 \times 2)$ Sn/Pt(111) surface alloy a comparatively high ethane selectivity in the low reaction temperature region and consequently a low methane selectivity in comparison to Pt(111) and the $(\sqrt{3} \times \sqrt{3})$R30° Sn/Pt (111) surface alloy.

Bond *et al.* (18) observed a very similar phenomenon in studying the *n*-butane hydrogenolysis on supported Pt/Al_2O_3 and Re–Pt/Al_2O_3 catalysts. They found that the addition of Re to the base Pt/Al_2O_3 catalyst resulted in a marked increase in ethane and decrease in propane selectivities. Somewhat surprisingly, at the lowest reaction temperature (530 K) the $p(2 \times 2)$ Sn/Pt(111) surface alloy shows higher propane than methane selectivity and the ethane selectivity is over 50%. We suggest that the selectivity pattern at low reaction temperatures derives from *n*-butane molecules adsorbing in two different reactive configurations on the $p(2 \times 2)$ Sn–Pt(111) surface. The dominant reactive adsorption geometry is the one in which *n*-butane is bound to the surface through its 2- and 3-carbon atoms which activates the internal C–C bond for hydrogenolysis. The resulting C_2H_y surface species are then hydrogenated off from the surface as ethane. The other adsorption configuration produces 1,2-adsorbed C_4H_z surface species and its terminal C–C bond breaking results in the formation of CH_x and C_3H_y surface species. At low reaction temperatures the C_3H_y surface species hydrogenates and leaves the surface as propane. Although not as likely, CH_x fragments could additionally react with the C_2H_v species, producing C_3 surface entities which can desorb as propane via further hydrogenation. This coupling mechanism could account for the high propane and low methane selectivities observed at low reaction temperatures. At higher temperatures this channel of propane formation is not operational and the selectivity for propane formation decreases rapidly, while the selectivity for methane formation increases sharply with increasing reaction temperature. The monotonic drops in ethane and propane selectivities with increasing reaction temperature suggest that at higher temperatures multiple C–C bond cleavages occur on the $p(2 \times 2)$ Sn/Pt(111) alloy surface. At 625 K predominately methane formation is seen with propane selectivity falling to 13%. Even with this high methane formation level the ethane selectivity is still over 30%. The observed selectivity patterns for the $p(2 \times 2)$ Sn/Pt(111) alloy surface strongly suggest that multiple hydrogenolysis events occur from two geometrically different adsorbed intermediate C_4 species at elevated temperatures. For the $(\sqrt{3} \times \sqrt{3})$R30° Sn/Pt(111) surface alloy the selectivity pattern is a lower ethane and higher methane production compared to the $p(2 \times 2)$ Sn/Pt(111) surface alloy over the entire temperature range studied. This suggests that the relative population of the 1,2-adsorbed C_4 species compared to the 2,3-adsorbed one is higher on the $\sqrt{3}$ surface that it is on the $p(2 \times 2)$ alloy. This would presumably result in a higher methane and lower ethane production even at low reaction temper-

atures. As seen on all of the surfaces multiple C–C cleavages occur resulting in sharp decreases in both the ethane and propane selectivities and a pronounced increase in methane selectivity.

B. Hydrogen Partial Pressure Dependence

The orders of the reaction rates of *n*-butane hydrogenolysis as well as the product distributions as a function of hydrogen partial pressure are notably different for the Pt(111) and Sn/Pt(111) systems. Figure 3 demonstrates that all three surfaces exhibit differing positive orders in hydrogen pressure dependence over a limited hydrogen partial pressure regime. Above a critical hydrogen pressure the reaction rate becomes independent of the hydrogen partial pressure. In addition, the product selectivities are essentially unchanged above these limiting hydrogen pressures for all three surfaces. However, the orders of the reaction rates in hydrogen pressure are significantly different for the three surfaces studied. The reaction rate over the $p(2 \times 2)$ Sn/Pt(111) alloy has a +1.6 order hydrogen pressure dependence, while the Pt(111) and $(\sqrt{3} \times \sqrt{3})$R30° Sn/Pt(111) catalysts give orders of +0.8 and +0.4, respectively. The hydrogen pressures where the rate rollovers occur is slightly different for the Pt(111) and Sn/Pt(111) surface alloys, being ~50 Torr for the two alloy surfaces and ~80 Torr for Pt(111). Similar behavior in catalytic activity as a function of hydrogen partial pressure has been observed previously in *n*-butane hydrogenolysis over Ir(111) (12). The referenced rollover behavior was rationalized by the depletion of surface hydrogen coverage at hydrogen pressures below the critical value. Following the argument for this prior work, at high hydrogen pressures the surface is saturated with adsorbed hydrogen atoms at the given reaction temperature and the kinetics are no longer influenced by the hydrogen adsorption process. Since the hydrocarbon fragment adsorption is strong, the overall reaction rate will have a zero order hydrogen pressure dependence above this critical hydrogen partial pressure. This critical hydrogen pressure is higher for the clean Pt(111) surface in accordance with the observed (4) weaker hydrogen adsorption on Pt(111) than on the Sn/Pt(111) alloys. As the hydrogen pressure drops below this limiting value the reaction rate decreases since the surface coverage of hydrogen decreases and the kinetics of the H_2 dissociation influence the reaction. The difference in the order of hydrogen partial pressure dependence may be rationalized by the differences in both the hydrocarbon and hydrogen adsorption strength and also by the differences in the adsorption configuration of the hydrocarbon molecules.

The product selectivities as a function of hydrogen partial pressure show behavior similar to that observed for TOFs as a function of hydrogen partial pressure. At hydrogen pressures higher than the above mentioned critical values the product selectivities are also constant. At high hydrogen pressure (100 Torr) the Pt(111) surface produces methane with ~60% selectivity, while the propane selectivity is only ~12%. This large difference between the methane and propane selectivities at high hydrogen partial pressures demonstrates that at Pt(111) multiple hydrogenolysis events occur. Decreasing the hydrogen pressure results in a decrease in methane formation and increases in both ethane and propane production; therefore, we can conclude that multiple hydrogenolysis events of *n*-butane on Pt(111) are not favored as the hydrogen partial pressure decreases. With decreasing hydrogen partial pressure the product selectivities continuously move toward the statistical distribution suggested by Davis *et al.* (16) for Pt(111).

The product selectivities for the $(\sqrt{3} \times \sqrt{3})$R30° Sn/Pt(111) surface alloy show a very similar pattern to that observed at Pt(111). For the $p(2 \times 2)$ Sn/Pt(111) surface alloy at high hydrogen partial pressures, i.e., constant activity regime, this catalyst produces about 50% ethane and 20 and 30% propane and methane, respectively. Below the critical hydrogen partial pressure the ethane selectivity over the $p(2 \times 2)$ Sn/Pt(111) surface alloy is lower than that observed for the two other surfaces studied, namely, with decreasing hydrogen pressure the ethane selectivity drops. Concomitantly, the propane selectivity increases sharply and reaches 35% at a hydrogen pressure of 10 Torr. At this low hydrogen pressure the amount of propane produced is significantly higher than that of methane. At high hydrogen pressures the surface is saturated with adsorbed hydrogen and the C_2H_x surface species produced by the central C–C bond breaking of adsorbed *n*-butane is readily hydrogenated and desorbs from the surface. On the $p(2 \times 2)$ Sn/Pt(111) surface we speculate that the concentration of the 1,2-adsorbed C_4 species is low; therefore, at high hydrogen pressures the amounts of methane and propane produced are correspondingly low. The slightly higher methane than propane selectivity can be attributed to a low extent of multiple hydrogenolysis. Below some critical surface hydrogen coverage the C_2H_x species are not hydrogenated rapidly enough (with subsequent rapid desorption) and, therefore, they can react with CH_y species increasing the amount of propane produced. The parallel decreases of the methane and ethane product selectivities as well as the sharp increase of the propane production are consistent with this mechanistic picture. The production of propane from the $p(2 \times 2)$ Sn/Pt(111) surface alloy seems to be easier at low hydrogen pressures than that of ethane. Perhaps a larger geometric strain expected from an adsorbed C_3 species than a C_2 entity may account for this result. We suggest that the stability of the C_2H_x species is significantly increased on the $p(2 \times 2)$ Sn/Pt(111) surface alloy compared to Pt(111).

C. Deactivation of Pt(111) and p(2 × 2) Sn/Pt (111)

The activity of the Pt(111) catalyst drops sharply with the number of reaction runs and concomitantly the amount of accumulated carbonaceous surface residues increases sharply. The activity of this catalyst in the second reaction cycle is less than 50% of the original activity and in the fifth run it drops below 10% of the initial value. The observed very fast deactivation of the Pt(111) catalyst has been reported earlier (19, 24) and can be completely accounted for by the accumulation of carbonaceous residues on the catalyst surface. The major role of these residues is to poison the reaction by blocking catalytically active reaction sites. Along with the change in catalytic activity the selectivity pattern is also altered by the deactivation. In every reaction run methane is produced with the highest selectivity; however, it is formed with increasing selectivity as the activity of the catalyst decreases. In the first reaction run methane is produced with 36% selectivity which increases to ~60% in the fifth reaction run. Meanwhile, the selectivities of both ethane and propane decrease and propane is formed with the lowest selectivity in each and every reaction run. This selectivity pattern suggests that with deactivation the role of multiple hydrogenolysis sharply increases. The deposition of carbon on the Pt(111) surface affects the electronic properties of surface Pt atoms in the opposite direction of that of Sn. The interaction between the hydrocarbon molecules and the surface Pt atoms is suggested to become stronger as carbon is deposited on the surface. This enhanced strength of hydrocarbon adsorption is responsible for the increased multiple C–C bond breaking and therefore for the increased selectivity toward methane production. Another plausible explanation for the increased methane production is that under reaction conditions a significant fraction of the carbonaceous deposits hydrogenate and leave the surface as methane. Not surprisingly, some deactivation was also seen for the $p(2 \times 2)$ Sn/Pt(111) surface alloy. The activity of the $p(2 \times 2)$ Sn/Pt(111) surface alloy decreases measurably with the number of reaction runs. The activity observed in the second run is half of that seen in the first cycle. However, this catalyst is still more active than a fresh clean Pt(111) surface, even after the fourth batch reaction. The origin of the observed sharp activity drop of the $p(2 \times 2)$ Sn/Pt(111) catalyst is not entirely understood. This dramatic decrease in activity can not be explained merely by the accumulation of surface carbonaceous residues since post-reaction surface AES analysis displayed barely any detectable carbon residue. The only change we observed in the catalyst surface after reaction came from postreaction LEED analysis. Before reaction the alloy surface provided a very sharp $p(2 \times 2)$ LEED pattern. However, even after the first reaction run the LEED picture became significantly less sharp and some very weak additional spots were seen which were characteristic of the $(\sqrt{3} \times \sqrt{3})R30°$ Sn/Pt(111) surface alloy structure. With increasing number of reaction runs the $\sqrt{3}$ spots became somewhat more intense, but their intensity never became comparable to that of the $p(2 \times 2)$ spots. It is conceivable that the very small amount of carbon deposited on the $p(2 \times 2)$ surface is responsible for the formation of catalytically much less active $\sqrt{3}$ domains, or that reaction conditions themselves drive this significant surface reconstruction. The carbon deposited during the catalytic reaction may compress the $p(2 \times 2)$ surface structure and create $\sqrt{3}$ domains. The small amount of carbon present after reaction runs and the changes in surface structure together might be responsible for the observed deactivation of the $p(2 \times 2)$ Sn/Pt(111) surface alloy. The product selectivities as a function of the number of reaction run over the $p(2 \times 2)$ alloy did not change as dramatically as was seen for the Pt(111) surface. There is only a very slight change in the methane selectivity, varying from 35–38%. The most noticeable change can be seen for the propane selectivity which increases rather significantly from 12% in the first reaction run to 23% in the seventh catalytic cycle. Correspondingly, the ethane production decreased somewhat, but it still remained the most abundant product. Both of the above-mentioned phenomena, the small amount of carbon deposition and the formation of $\sqrt{3}$ domains, could account for the decrease of ethane selectivity and an increase in propane selectivity.

SUMMARY

The overall conclusion of the examination of n-butane hydrogenolysis reactivity using ordered Sn/Pt(111) bimetallic surfaces are that increased activity, marked selectivity changes, and resistance to catalytic deactivation can all be obtained. These reactivity changes are attributed to ensemble restrictions (number of contiguous Pt atoms), steric strain from surface rippling, and electronic surface modifications brought about by alloying. These effects are all closely coupled and have been measured in related, independent surface characterization studies.

REFERENCES

1. Sinfelt, J., Bimetallic Catalysts, Exxon Mono. Series, Wiley, New York, 1983.
2. Ku, Y-S., and Overbury, S. H., *Surf. Sci.* **273,** 353 (1992).
3. Li, Y. D., Jiang, L. Q., and Koel, B. E., *Phys. Rev. B,* submitted for publication.
4. Paffett, M. T., and Windham, R. G., *Surf. Sci.* **208,** 34 (1989).
5. Paffett, M. T., Logan, A. D., Simonson, R., and Koel, B., *Surf. Sci.* **250,** 123 (1991).
6. Overbury, S. H., Mullins, D., Paffett, M. T., and Koel, B. E., *Surf. Sci.* **254,** 45 (1991).

7. Ferro, R., Capelli, R., Borese, A., and Delfino, S., *Atti Accad. Naz. Lincei Cl. Sci. Fis. Mat. Nat. Rend.* **54,** 634 (1973).
8. Hultgren, R., Orr, R. L., Anderson, P. D., and Kelley, K. K., "Selected Values of Thermodynamic Properties of Metals and Alloys," Wiley, New York, 1963.
9. Bond, G. C., "Proceedings, 10th International Congress on Catalysis, Budapest, 1992" (L. Guczi, F. Solymosi, and P. Tetenyi, Eds.). Akadémiai Kiadó, Budapest, 1993.
10. Nazimek, D., and Ryczkowski, J., *Appl. Catal.* **26,** 47 (1986).
11. Anderson, J. R., and Avery, N. R., *J. Catal.* **5,** 446 (1966).
12. Engstrom, J. R., Goodman, D. W., and Weinberg, W. H., *J. Am. Chem. Soc.* **110,** 8305 (1988).
13. Kalakkad, D., Anderson, S. L., Logan, A. D., Pena, J., Braunschweig, E. J., Peden, C. H. F., and Datye, A., *J. Phys. Chem.* **97,** 1437 (1993).
14. Logan, A. D., and Paffett, M. T., "Proceedings, 10th International Congress on Catalysis, Budapest, 1992" (L. Guczi, F. Solymosi, and P. Tetenyi, Eds.). Adadémiai Kiadó, Budapest, 1993.
15. Campbell, C. T., and Paffett, M. T., *Surf. Sci.* **139,** 396 (1984).
16. Davis, S. M., Zaera, F., and Somorjai, G. A., *J. Am. Chem. Soc.* **104,** 7453 (1982).
17. Bond, G. C., Garin, F., and Maire, G., *Appl. Catal.* **41,** 313 (1988).
18. Bond, G. C., and Gelsthorpe, M. R., *J. Chem. Soc., Faraday Trans. I* **85**(11), 3767 (1989).
19. Davis, S. M., Zaera, F., and Somorjai, G. A., *J. Catal.* **85,** 206 (1984).
20. Kempling, J. C., and Anderson, R. B., *Ind. Eng. Chem. Process Des. Dev.* **9**(1), 116 (1970).
21. Bond, G. C., and Paal, Z., *Appl. Catal. A: General* **86,** 1 (1992).
22. Xu, C., Koel, B. E., and Paffett, M. T., *Langmuir* **10,** 166 (1994).
23. Sault, A., and Goodman, D. W., *J. Chem. Phys.* **88,** 7232 (1988).
24. Coq, B., and Figueras, F., *J. Catal.* **85,** 197 (1984).
25. Coq, B., and Figueras, F., *J. Mol. Catal.* **25,** 87 (1984).
26. Burch, R., and Garla, L. C., *J. Catal.* **71,** 360 (1981).
27. Burch, R., *Acc. Chem. Res.* **15,** 24 (1982).
28. Darpinski, Z., and Clarke, J. K. A., *J. Chem. Soc., Faraday Trans. I* **71,** 893 (1975).
29. Paffett, M. T., Gebhard, S. C., Windham, R. G., and Koel, B. E., *Surf. Sci.* **223,** 449 (1989).
30. Sachtler, W. M. J., and Somorjai, G. A., *J. Catal.* **81,** 77 (1983).